International Journal for Housing Science and Its Applications
Publish August 10, 2025. Volume 46, Issue 4 Pages 7265-7283

https://doi.org/10.70517/ijhsa464630

Research on transformer operation status monitoring methods based on acoustic signal analysis: Taking substations in urban building complexes as an example

Yaguo Li[1], Lijun Feng[1], Ruirong Li[1,*], Xi Cui[1] and Jun Li[1]
[1] State Grid Shanxi Electric Power Company Yuncheng Power Supply Company, Yuncheng, Shanxi, 044000, China
Corresponding authors: (e-mail: lrr348591487@163.com).

Abstract This study addresses the challenge of transformer condition monitoring in the complex electromagnetic environment of urban building complexes by proposing an intelligent diagnostic method based on acoustic signature signal analysis. Through electromagnetic-mechanical coupling theory analysis, the study clarifies the acoustic signature generation mechanisms of winding vibration and core magnetostriction, and reveals the resonance risks caused by harmonic interference. A multi-channel high-speed synchronous data acquisition system is designed, integrating high-precision sensors and FPGA modules to collect vibration data from an 110kV transformer. An improved EEMD denoising algorithm is proposed, utilizing minimum cutoff frequency constraints and multi-sensor fusion strategies to enhance noise suppression performance. Based on the denoised acoustic signature features, an SSAE-IELM fault diagnosis model is constructed, with incremental extreme learning machines enabling rapid classification. Experiments show that the improved CEEMD algorithm achieves a signal-to-noise ratio of 18.11 dB, an improvement of 26% over EEMD, with the mean square error reduced to 0.0177 and computational efficiency improved by one-third. In transformer fault identification tests across four states (normal, short-circuit impact, DC bias, and partial discharge), the model achieves an accuracy rate of 94.11%, significantly outperforming CNN's 82.46%.

Index Terms urban building complex substation, acoustic signature signal, transformer; operational monitoring, EEMD, SSAE-IELM

I. Introduction

As urban electricity demand continues to grow, substations play a crucial role as an essential component of the power system within urban building complexes [1], [2]. A substation is a facility within the power system primarily used to convert high-voltage electricity into low-voltage electricity, while also performing functions such as control, protection, metering, and monitoring of electrical energy to meet requirements for power transmission, distribution, supply, and other related needs [3]-[6]. The most important equipment in a substation is the transformer, whose primary function is to convert the high-voltage electricity transmitted to the substation into low-voltage electricity to meet various power requirements [7]-[9]. With the continuous development of power equipment technology, transformers, as important equipment in power systems, have become increasingly significant in power systems [10], [11]. However, due to factors such as complex working environments, large load variations, and susceptibility to influences from other power system equipment, transformers have a high failure rate. Therefore, monitoring and analyzing the operational status of transformers is of great significance for improving the reliability and stability of power systems [12]-[15].

To achieve real-time monitoring of transformer operational status and improve the accuracy and efficiency of fault diagnosis, acoustic signature analysis has emerged as a non-invasive, real-time monitoring method [16]-[18]. Acoustic signature analysis is based on acoustic signal analysis, which records sound fluctuations within the transformer to obtain critical information about its operational status and performance [19]-[21]. This monitoring method not only eliminates the need for shutdown or disassembly of the transformer but also enables real-time data acquisition during operation, providing an efficient and feasible means for power system health management [22]-[24]. However, to fully leverage the potential of acoustic signal analysis, it is necessary to conduct in-depth research on its application characteristics, monitoring objectives, and data processing methods in hydroelectric power station transformers [25]-[27].

Reference [28] investigated the acoustic signature characteristics of vibration acoustic signals under different operating conditions in transformers. By constructing an automatic non-invasive monitoring and fault diagnosis

system for transformers based on acoustic features, it was verified that the system can rapidly identify fault operating conditions with very high accuracy. Reference [29] investigated transformer condition diagnosis based on acoustic signals and proposed an abnormal diagnosis method for power transformers using an Attention-CNN-LSTM hybrid model to enhance the accuracy and efficiency of acoustic anomaly diagnosis methods. The results demonstrated that this model effectively improved the accuracy of transformer condition acoustic detection. Literature [30] discusses transformer operational detection and anomaly diagnosis, and investigates the application of AI-based sound recognition technology in transformer discharge diagnosis, aiming to enhance the diagnostic capabilities of intelligent monitoring systems for substation equipment. Literature [31] collected transformer acoustic signature signals under three operating conditions—loaded, lightly loaded, and unloaded—using an acoustic signature signal acquisition platform, and proposed a pattern recognition method based on the RUSBoost algorithm. The research results provide a reference for utilizing sample-imbalanced acoustic signature monitoring and recognition to assess the mechanical state of transformers. Literature [32] emphasizes the important role of transformers in power systems and the numerous fault challenges they face, which can affect their normal operation. Based on this, examining condition monitoring and fault diagnosis technologies for large transformers in use can help with real-time handling of transformer faults and ensure their normal operation. Literature [33] introduces the application of acoustic signature signals in transformer fault diagnosis and the challenges it faces, and proposes a fault diagnosis method that considers both continuous noise and transient noise. Through experiments, it verifies that this method can quickly and accurately identify the operational status of transformers, with very high identification accuracy in various complex environments. Literature [34] proposes a transformer fault diagnosis method based on small-sample acoustic fingerprint recognition technology. By extracting the operational characteristics of transformers based on the principles of acoustic fingerprint recognition technology, the method compares and classifies transformer fault acoustic fingerprints, revealing that it possesses excellent recognition accuracy and holds significant practical engineering implications. Literature [35] introduces a fault diagnosis method for power transformer acoustic signals based on hybrid data augmentation and convolutional neural networks, and verifies that this method achieves very high accuracy in diagnosing typical power transformer unbalanced faults. Literature [36] reviews various diagnostic methods for power transformer operational status, such as partial discharge, temperature, and optical detection, analyzes the advantages and disadvantages of different monitoring methods, and emphasizes the technical challenges and future development prospects of transformer optical monitoring methods. Reference [37] emphasizes the necessity of improving the situational awareness model for transformers, pointing out that current transformer state sensing technology has issues such as poor temporal effectiveness, and establishes a transformer state transition model based on Markov chain principles, verifying the effectiveness of this method, which plays an important role in transformer state early warning. Literature [38] proposes an intelligent fault diagnosis method for transformers based on multi-source data fusion and correlation analysis, aiming to achieve predictive maintenance and health management of transformers. Through experiments, the effectiveness of this method is demonstrated, enabling its application in accident prediction to ensure safe operation of transformers. Literature [39] describes temperature as the most important characteristic reflecting transformer faults. By analyzing multiple transformer parameters, the study combines pattern recognition with statistical analysis for early warning of potential hazards in transformers, emphasizing the method's ability to detect abnormal temperatures in transformers in advance. Literature [40] introduces the application of the Transformer Health Monitoring System (THMS) in real-time assessment of transformer performance and reviews the latest advancements in transformer technology. The study indicates that THMS contributes to enhancing the system safety of distribution networks by reducing manual inspections and enabling early fault detection. The above studies emphasize the importance of transformers in power systems, pointing out that transformers can fail due to environmental influences, thereby affecting the safe operation of power systems. Therefore, methods based on acoustic signature signals, convolutional neural networks, and small-sample acoustic signature recognition technology are proposed for detecting transformer operating conditions to ensure safe operation.

This paper takes urban substations as the scenario and proposes a comprehensive acoustic fingerprint monitoring methodology system, covering signal generation mechanisms, data acquisition system design, noise processing, and intelligent fault diagnosis. This provides new insights for assessing transformer status in complex electromagnetic environments. First, the paper thoroughly analyzes the mechanism of acoustic signal generation. Based on the electromagnetic-mechanical coupling theory, it derives the winding vibration equation and the core magnetostriction model, revealing the generation mechanism of the 100Hz fundamental frequency and its harmonic multiples, and clarifying the core issue of harmonic interference leading to resonance risks. Based on this, the acoustic signature acquisition system architecture is designed. Considering the high background noise levels at urban substations, the system integrates high-precision sensors, FPGA logic control modules, and a host computer to achieve multi-channel high-speed synchronous acquisition. An improved EEMD denoising algorithm is proposed,

employing minimum cutoff frequency constraints and multi-sensor fusion strategies to effectively suppress harmonic and white noise interference, addressing the limitations of traditional methods such as modal aliasing and low computational efficiency. An SSAE-IELM intelligent diagnostic model is established. A stacked sparse autoencoder is used to extract deep acoustic signature features, overcoming the bottlenecks of complex parameter tuning and slow convergence in traditional neural networks.

II. Mechanism of transformer acoustic signal generation and construction of operational status monitoring system

II. A. Mechanism of transformer acoustic signal generation

II. A. 1) Transmission path of transformer acoustic signal

The acoustic signature signals of a transformer are generated by vibrations in its internal structure. By analyzing these acoustic signature signals, operational information about the transformer can be obtained. However, due to the complex operating environment of transformers, a significant amount of DC components and harmonic components are introduced during operation, resulting in more complex time-frequency characteristics. Transformer vibrations primarily originate from the following factors: (1) core vibrations caused by the magnetostriction of silicon steel sheets; (2) winding vibrations caused by electromagnetic forces; (3) vibrations generated by the operation of cooling devices. Mechanical waves are transmitted through transformer oil and rigid connection components to the housing, then propagate outward through the air, forming specific acoustic signals. The vibration propagation path is illustrated in Figure 1.

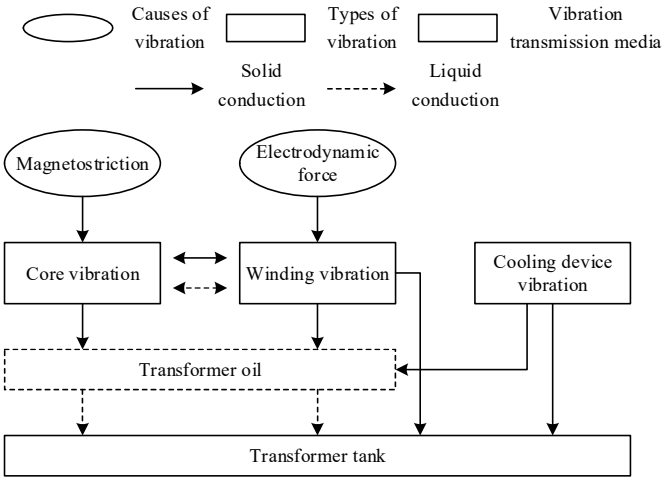

Figure 1: Transmission Path of Converter Transformer Vibration

II. A. 2) Mechanism of transformer winding vibration

The vibration of the winding originates from the electromagnetic force generated by the current flowing through the winding. According to the principles of high-voltage direct current transmission, during normal operation, the transformer's winding contains not only the rated current but also a significant amount of harmonic currents of orders $6k+1(k=1,2,3\cdots)$. Under the combined influence of the current and the multi-frequency magnetic field, vibration is generated. Let the current flowing through the winding be:

$$i=\sum_a I_{am}\cos\left(\alpha\omega_f t+\Phi_a\right) \tag{1}$$

In the equation, i — winding current/A, I_{am} — current amplitude/A, ω_1 — power frequency/Hz, Φ_α — current phase angle.

The interaction between currents and magnetic fields at different frequencies generates axial and radial electromagnetic forces, as shown in Equation (2). Under the influence of these electromagnetic forces, the winding undergoes vibration.

$$\begin{aligned} F_a &= k_{fa}\left(\sum I_{am}\cos\left(\alpha\omega_f t+\Phi_a\right)\right)^2 \\ F_r &= k_{fr}\left(\sum I_{am}\cos\left(\alpha\omega_f t+\Phi_a\right)\right)^2 \end{aligned} \tag{2}$$

In the equation, F_a and F_r — axial and radial electromagnetic forces on the winding / N, k_{fa} and k_{fr} — axial and radial electromagnetic force coefficients.

Based on the mechanical structure of the winding, it can be equivalently modeled as a spring-mass system, with the winding motion equation given by:

$$Ma + Cv + Kx = F \tag{3}$$

In the equation, M — mass matrix, C — damping coefficient matrix, K — elastic sparse matrix, F — electromagnetic force matrix, a, v, x — acceleration, velocity, and displacement matrices, respectively.

According to equation (3), the axial acceleration and radial acceleration of the winding are calculated separately, omitting the decay term, and can be expressed as:

$$\begin{aligned} a_a &= k_{aa}\left(\sum p_1 I_{am}{}^2 \cos\left(2\alpha\omega_1 t + \varphi_1\right)\right. \\ &\quad + \sum\nolimits_b p_2 I_{\alpha_1 m} \cos\left(\left(\alpha_1 + \alpha_2\right)\omega_1 t + \varphi_2\right) \\ &\quad \left. + \sum\nolimits_2 p_3 I_{\alpha_1 m} I_{\alpha_2 m} \cos\left(\left(\alpha_1 - \alpha_2\right)\omega_1 t + \varphi_3\right)\right) \\ a_r &= k_{ar}\left(\sum p_1 I_{\alpha m}{}^2 \cos\left(2\alpha\omega_1 t + \varphi_1\right)\right. \\ &\quad + \sum\nolimits_b p_2 I_{\alpha_1 m} \cos\left(\left(\alpha_1 + \alpha_2\right)\omega_1 t + \varphi_2\right) \\ &\quad \left. + \sum\nolimits_b p_3 I_{\alpha_1 m} I_{\alpha_2 m} \cos\left(\left(\alpha_1 - \alpha_2\right)\omega_1 t + \varphi_3\right)\right) \end{aligned} \tag{4}$$

In the equation, a_a and a_r — axial and radial acceleration/$\mathrm{m \cdot s^{-2}}$, k_{aa} and k_{ar} — acceleration coefficients, p_1, p_2, p_3 — calculation parameters, φ_1, φ_2, φ_3 — acceleration phase angles/rad.

From equation (4), it can be seen that under ideal conditions, considering only the power frequency current, the fundamental frequency of the winding vibration acceleration is 100 Hz. However, when the transformer is operating, there are a large number of harmonics. Under the influence of harmonic currents, in addition to the 100 Hz component, the vibration acceleration also clearly contains 100 kHz components, with a wide frequency distribution. When the natural frequency of the winding is close to this, resonance is likely to occur, causing the main vibration frequency to deviate from 100 Hz. Additionally, the large number of 100 Hz harmonic components will exacerbate vibration noise, making acoustic diagnosis challenging.

II. A. 3) Vibration Mechanism of Transformer Core

The primary cause of transformer core vibration is similar to that of ordinary power transformers, both originating from the magnetostriction of silicon steel sheets. To reduce eddy current losses, the core is constructed from multiple layers of silicon steel sheets stacked together, combined with stepped joints and non-woven adhesive tape technology. The core vibration is primarily equivalent to magnetic strain vibration. Magnetic strain is an inherent property of ferromagnetic materials under the influence of an external magnetic field, manifesting as reversible changes in length or volume. During normal operation of the transformer, the magnetic field strength does not reach saturation, so the magnetic strain phenomenon primarily manifests as minor changes in length. Figure 2 illustrates the magnetic strain phenomenon of silicon steel sheets from a microscopic perspective. When no external magnetic field is present, the total magnetic moment is zero, and magnetic domains are randomly distributed within the ferromagnetic material, showing no obvious pattern. When an external magnetic field is present, the magnetic domains are displaced by the magnetic field, causing changes in magnetic spacing, which result in alterations to the length of the silicon steel sheets.

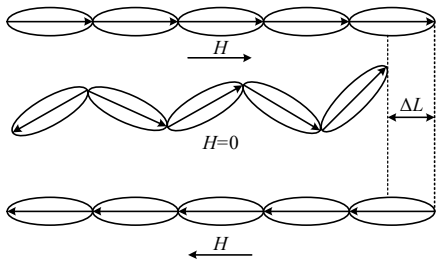

Figure 2: Magneto strictive Effect

Next, we will analyze the vibration mechanism of the transformer core. Let us assume that the ideal voltage of the transformer is:

$$u(t) = U \sin \omega t \tag{5}$$

In the formula, u ——transformer voltage/V, U ——fundamental wave amplitude/V.

The voltage and magnetic induction intensity in the core have the following relationship:

$$u(t) = -N_1 A_c \frac{dB}{dt} \tag{6}$$

In the formula, N_1 ——number of turns in the primary winding/turn, A_c ——cross-sectional area/cm².

According to formulas (5) and (6), we have:

$$B = -\frac{U}{N_1 A_c} \int \sin \omega t dt = \frac{U}{N_1 A_c \omega} \cos \omega t = B_0 \cos \omega t \tag{7}$$

During normal operation, the magnetic flux in the core is less than the saturation magnetic flux density of the ferromagnetic material. At this point, the saturation magnetic flux density B_s is linearly related to the coercive force strength H_c:

$$B_s = \mu H_c \tag{8}$$

In the formula, B_s ——saturated magnetic flux density/T, H_c ——coercive force field strength/$\mathrm{A/m}$, μ ——core magnetic permeability/$\mathrm{H/m}$.

Then the core magnetic induction intensity H can be expressed as:

$$H = \frac{B}{B_s} H_c = \frac{B_0}{B_s} \cos \omega t \tag{9}$$

The magnitude of magnetic strain in the core can be expressed by the magnetic strain coefficient δ:

$$\delta = \frac{\Delta L}{L} \tag{10}$$

In the formula, ΔL ——Deformation length under magnetostriction/cm, L ——Original length of silicon steel sheet/cm.

According to formula (10), we can obtain:

$$\Delta L = L\delta = \frac{L\delta U^2}{\left(N_1 A_c \omega B_s\right)^2} \cos^2 \omega t \tag{11}$$

The vibration acceleration of the iron core can be expressed as:

$$a = \frac{d\left(\Delta L\right)^2}{dt^2} = -\frac{2L\delta U^2}{\left(N_1 A_c B_s\right)^2} \cos 2\omega t \tag{12}$$

From equation (12), it can be seen that under the action of power frequency voltage, the main frequency of core vibration is 100 Hz, which is proportional to the square of the voltage.

During normal operation, transformers contain a large amount of harmonic voltage in addition to power frequency voltage. Therefore, their magnetic induction strength can be expressed as:

$$B(t) = B_0 \cos \omega t + \sum\nolimits_{am} B_\alpha \cos \alpha \omega t \tag{13}$$

In the formula, B_α ——Harmonic voltage magnetic induction intensity amplitude/T, B_0 ——Fundamental wave magnetic induction intensity amplitude/T.

In summary, the transformer core vibration acceleration is:

$$a=\frac{d\left(\Delta L\right)^2}{dt^2}=-\frac{2L\delta U^2}{\left(N_1A_cB_s\right)^2}\cos 2\omega t \\ -\sum\nolimits_{am}\left(\frac{2\alpha^2L\delta\omega^2B_k^2}{B_s^2}\cos 2\alpha\omega t\right) \tag{14}$$

From equation (14), it can be seen that the dominant frequency of core vibration is mainly 100 Hz, and harmonic voltage effects will bring more 100 Hz harmonic components. However, due to the nonlinearity of the core and other factors, the vibration may deviate, and the frequency components may be more complex.

II. B. Overall framework of the transformer acoustic fingerprint acquisition system

The above mechanism analysis indicates that transformer acoustic signature signals contain rich mechanical state information; however, harmonic interference in the complex electromagnetic environment of urban substations can significantly affect signal characteristics. Therefore, it is necessary to construct a high-precision data acquisition system to obtain raw acoustic signature data.

This paper primarily investigates transformer acoustic signature acquisition systems, which are mainly used for collecting sound signals emitted by transformers (or other power equipment) during operation, with the aim of constructing a high-precision, high-speed acoustic signature acquisition system. The acoustic signature acquisition system primarily consists of acoustic sensors, signal conditioning circuits, analog-to-digital converters (ADCs), logic control modules (FPGAs), and host computers.

II. C. Transformer acoustic signal data preprocessing method—improved EEMD algorithm

The raw acoustic signals obtained by the acquisition system inevitably contain environmental noise and electromagnetic interference, and direct diagnosis will lead to misjudgment. Therefore, this section proposes an improved EEMD denoising algorithm, which realizes noise separation and signal reconstruction through multi-sensor fusion and adaptive cutoff frequency design.

II. C. 1) Improvements to the EEMD Algorithm

Since EEMD repeatedly adds Gaussian white noise and performs multiple empirical mode decompositions, although it solves the problem of modal aliasing, it is prone to introducing false IMF components, and “overdecomposition” increases the computational load. Therefore, it is necessary to improve the computational efficiency of the EEMD method, i.e., the IMF screening termination condition problem. By applying a low-pass filter to the white noise signal, a band-limited noise signal can be obtained. Setting the cutoff frequency of the desired signal as the upper limit effectively eliminates modal aliasing in the low-frequency range and is more efficient than the traditional EEMD method. Based on the concept of cutoff frequency, this paper proposes an improved EEMD denoising algorithm with a minimum lower cutoff frequency. The specific steps are as follows:

(1) Assume that the raw acoustic signals collected by each acoustic sensor are $x_i(t)$, where $i=1,2,\cdots,M$ and M is the number of sensors. Perform short-time Fourier transform power spectrum analysis on $x_i(t)$ to identify the lowest frequency in the spectrum of the raw acoustic signal from each sensor as the cutoff frequency for signal decomposition corresponding to that sensor, and use it as the lower limit for signal decomposition, denoted as f_L.

(2) Add a Gaussian white noise sequence $h_k(t)$ with a mean of 0 and a standard deviation of 0.05 to 0.1 times the standard deviation of the original signal to each $x_i(t)$ to obtain the new signal $X_{i,k}(t)$, i.e.

$$X_{i,k}(t)=x_i(t)+h_k(t) \tag{15}$$

(3) $X_{i,k}(t)$ is used for EMD decomposition, taking $X_{1,1}(t)$ as an example, and the power spectrum of each order of IMF components $C_{1,j}(t)$ is analyzed again to obtain its main frequency $f_{\max}$, and $f_{\max}$ is compared with f_L, if $f_{\max}$ is less than f_L, the decomposition terminates, and conversely, the decomposition continues. Finally, the N order IMF component $C_{1,1},C_{1,2},\cdots,C_{1,N}$ is obtained after the EMD decomposition of $X_{1,1}(t)$. The same operation is performed on each $X_{i,k}(t)$ as that of $X_{1,1}(t)$ to obtain the IMF component group after a noisering.

(4) Repeat steps (2) and (3) K times to obtain K sets of IMF components. Calculate the overall average $C_{i,j}$ of the IMF components from the K decompositions to obtain the IMF components from the final EEMD decomposition of each voice sensor signal $X_i(t)$, i.e.,

$$C_{i,j} = \frac{1}{K}\sum_{s=1}^{K} C_{i,j,s}, i = 1,2,\cdots,M; j = 1,2,\cdots,N \tag{16}$$

(5) Calculate the correlation coefficients between each IMF component and the source signal separately. If the correlation coefficient of an IMF component is small, it indicates that the component contains a large amount of noise and should be discarded. Conversely, if the correlation coefficient is large, the component should be retained.

$$\rho_k = \frac{\sum_{t=1}^{K}\left(r_k(t)-\overline{r}\right)\left(x_k(t)-\overline{x}\right)}{\sqrt{\sum_{t=1}^{K}\left(r_k(t)-\overline{r}\right)^2}\sqrt{\sum_{t=1}^{K}\left(x_k(t)-\overline{x}\right)^2}} \tag{17}$$

where ρ_k, $k = 1,2,\cdots,K$ are the IMF correlation coefficient values obtained for each order, $r(t)$ represents the IMF component, $\overline{r}$ is the average value of $r(t)$, $x(t)$ represents the transformer sound signal, and $\overline{x}$ is the average value of $x(t)$. and K denotes the order of the IMF component.

(6) By setting a reasonable threshold μ, IMF components with correlation coefficient values greater than the threshold are retained, while those below the threshold are discarded.

$$\mu = \sqrt{\frac{\sum_{k=1}^{K}(\rho_k - \overline{\rho})}{K}} \tag{18}$$

where $\overline{\rho}$ is the average value of ρ.

(7) The noise-reduced sound signal of the transformer is obtained by superimposing the retained IMF components.

II. C. 2) Improved EEMD denoising based on multi-sensor fusion

Multi-sensor data fusion is applied to the acoustic array. A consistency-based data fusion algorithm is used to identify each sensor, discard faulty sensors, determine the valid sensor group, and complete data preprocessing. An improved EEMD based on the minimum lower frequency cutoff is used to denoise the acquired data from the valid sensor group. The effective IMF components are selected using the correlation coefficient method, and the denoised signal is reconstructed by superimposing the effective IMF components. The proposed improved EEMD-based noise reduction process for transformer acoustic signals using multi-sensor fusion is shown in Figure 3.

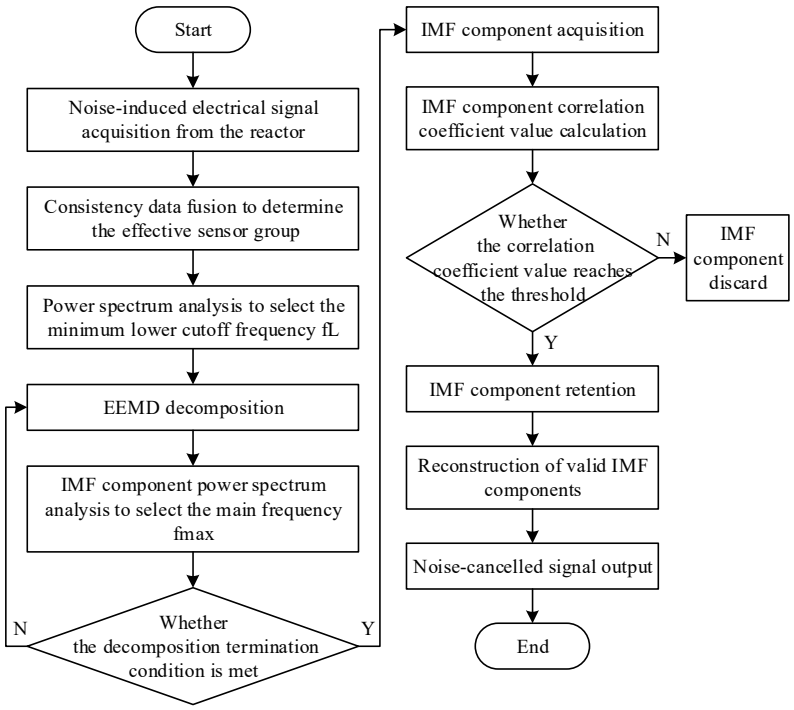

Figure 3: Improved EEMD Transformer Sound Signal Denoising Process

II. D.Acoustic diagnosis method for transformer mechanical faults based on SSAE-IELM

This section introduces the SSAE-IELM model, which establishes a mapping relationship between voiceprint features and fault types through deep feature extraction and incremental learning mechanisms.

II. D. 1) Transformer fault diagnosis model based on SSAE-IELM

The time-frequency energy matrix obtained after preprocessing still suffers from high dimensionality and excessive redundant information. Additionally, it is challenging to establish a mapping relationship between the time-frequency energy matrix and the mechanical state of the transformer solely through the matrix. Therefore, it is necessary to perform deep feature extraction on the time-frequency energy matrix of the transformer's acoustic signals and then utilize a fault identification model to establish a mapping relationship between the acoustic signals and the mechanical state of the transformer. However, traditional manual feature extraction methods suffer from drawbacks such as strong subjectivity, easy loss or redundancy of feature information, which affect the accuracy of subsequent fault identification results. The unsupervised self-learning mechanism of autoencoder networks can efficiently extract deep acoustic features of transformers through encoding and decoding processes, minimizing the loss of acoustic features. Additionally, transformer acoustic features exhibit characteristics such as strong ambiguity and minimal differences between features. When using traditional neural networks like BP neural networks or support vector machines to identify transformer mechanical states, issues such as low computational efficiency, complex parameter tuning, and non-convergent computational results may arise. To deeply analyze the correlation between transformer acoustic features and mechanical states, an incremental extreme learning machine (SSAE-IELM) is used to replace traditional neural networks. This approach fully explores the differences in acoustic features under various mechanical states, efficiently and quickly establishing a mapping relationship between transformer acoustic features and mechanical states, thereby improving the computational speed and accuracy of acoustic diagnosis for transformer mechanical faults.

This section introduces the basic principles and network structure of the stacked sparse autoencoder and incremental extreme learning machine (SSAE-IELM), and constructs a transformer mechanical fault identification model based on the SSAE-IELM network. The SSAE network's unsupervised self-learning is used to extract transformer acoustic features, and the IELM network's supervised training is employed to achieve intelligent diagnosis of transformer mechanical faults.

II. D. 2) Transformer fault diagnosis steps based on SSAE-IELM

Building on the transformer sound signal preprocessing discussed in Section 2.3, the transformer mechanical fault acoustic diagnosis model proposed in this section, based on a stacked sparse autoencoder and incremental extreme learning machine (SSAE-IELM) network, primarily consists of the following three components: First, the transformer sound signal is decomposed using the complementary empirical mode decomposition algorithm to calculate the signal's time-frequency energy matrix; Second, based on transformer sound data under different mechanical states and the unsupervised self-learning mechanism of the stacked sparse autoencoder network, deep acoustic features of the transformer sound signals are extracted. Additionally, the stacked sparse autoencoder network is trained through supervised learning using sound data labels to achieve fine-tuning and optimization of network parameters; Third, based on transformer acoustic features and the supervised learning mechanism of incremental extreme learning machines, establish a mapping relationship between transformer acoustic features and mechanical states to achieve intelligent identification of transformer mechanical faults. The acoustic diagnosis steps for transformer mechanical faults based on SSAE-IELM are as follows:

(1) Use the sound acquisition system to obtain transformer sound signals;

(2) Decompose the transformer sound signals using the complementary set empirical mode decomposition algorithm to obtain the intrinsic mode components with time-frequency features of the signal;

(3) Calculate the instantaneous frequency of the intrinsic mode components of the sound signals using the Hilbert transform, and reconstruct the intrinsic mode components into new signals by bandpass filtering according to the frequency bands, thereby obtaining the time-frequency matrix of the reconstructed signals;

(4) Calculate the time-frequency energy matrix of the reconstructed signal to obtain a one-dimensional time-frequency energy vector of the transformer sound signal;

(5) Use the SSAE network to perform deep feature extraction on the time-frequency energy vector of the transformer sound signal to obtain the acoustic fingerprint features of the signal, which are then used as the acoustic fingerprint dataset;

(6) Divide the transformer acoustic fingerprint dataset proportionally into training and testing sets. Use the acoustic fingerprint training set to train and optimize the network parameters of the IELM classification model, and validate the performance of the trained IELM classification model using the acoustic fingerprint testing set.

In summary, the steps for transformer mechanical fault acoustic diagnosis based on SSAE-IELM are shown in Figure 4.

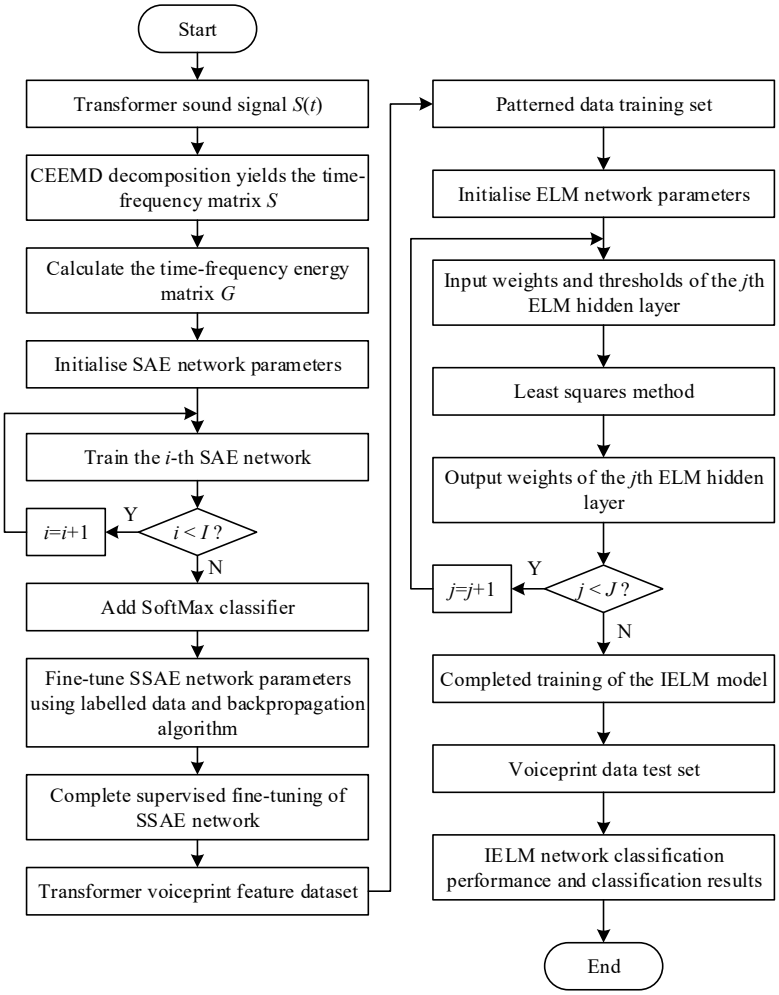

Figure 4: Steps for Acoustic Diagnosis of Mechanical Failures Based on SSAE-IELM

III. Analysis of transformer vibration signals based on improved EEMD denoising

Chapter 2 provides an in-depth analysis of the generation mechanism of transformer acoustic signals and the design of the acquisition system, and proposes improvements to the EEMD denoising and SSAE-IELM diagnostic models. Based on the above theoretical framework, Chapter 3 focuses on practical applications, first verifying the reliability of the acoustic signal acquisition system through actual measurement data, then analyzing the time-frequency characteristics of the signals, and finally combining the improved CEEMD algorithm to achieve denoising of vibration signals and performance comparison.

III. A. Transformer measurement data collection and preprocessing

In July 2024, a study was conducted at a certain substation to collect vibration data from 110kV transformers. The transformer acoustic fingerprint collection system and intelligent transformer vibration monitoring terminal designed in Chapter 2 of this paper were used to collect high-voltage side vibration signals from multiple transformers. During the data collection process, the six sensors of the monitoring terminal were placed in close contact with the surface of the transformer oil tank. In accordance with the safety regulations of the substation, the sensors were uniformly distributed on the surface of the oil tank at positions below half the height, with equal intervals, and data was continuously collected over several days.

The data collection period for the normal data used in this experiment was from July 10 to July 16, 2024. Channels 1 to 6 of Transformer No. 4 were selected as the experimental samples, with the data collected over the first five days serving as the training set, the data collected on the sixth day as the validation set, and the data collected on

the seventh day as the test set. Additionally, acoustic vibration data under DC bias conditions was collected from Transformer No. 6. Considering the actual operating environment of the transformer, two types of abnormal signals were generated based on the normal signal: abnormal signals with added noise and abnormal signals with added high-frequency harmonics. Figure 5 shows the normal vibration waveform of transformer No. 4, Figure 6 shows the DC bias vibration waveform of transformer No. 6, Figure 7 shows the vibration waveform after adding noise to the abnormal signal, and Figure 8 shows the vibration waveform of the transformer with added high-frequency harmonic signals.

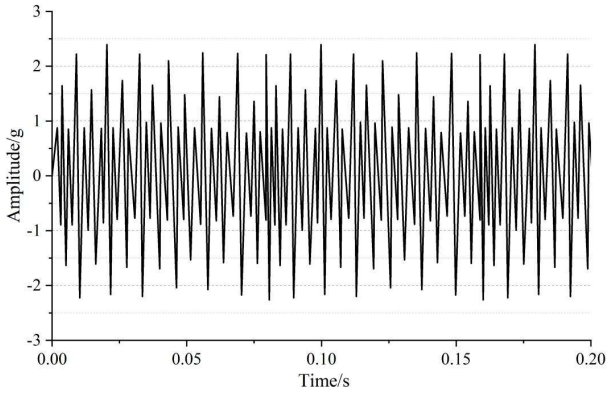

Figure 5: Normal vibration waveform of Transformer No. 4

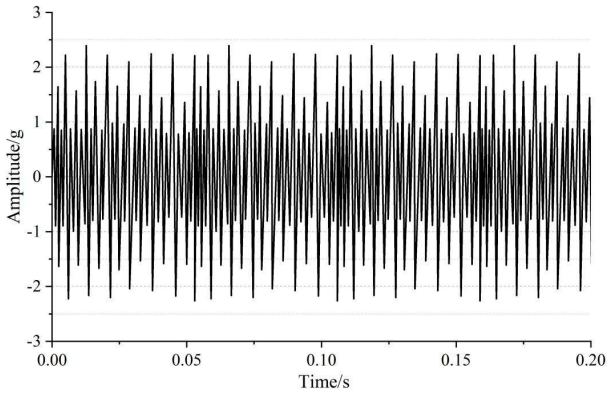

Figure 6: The DC bias-induced vibration waveform of the No. 6 transformer

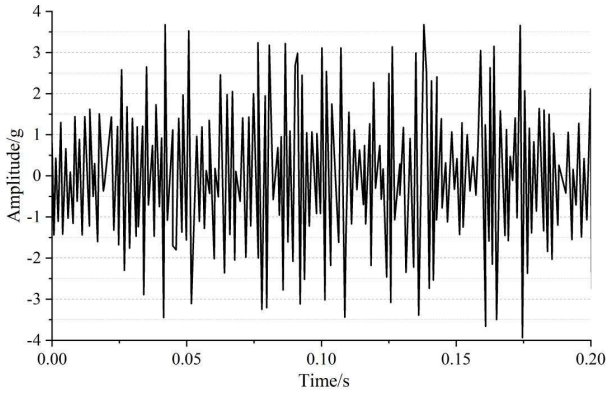

Figure 7: The vibration waveform after adding abnormal noise to the signal

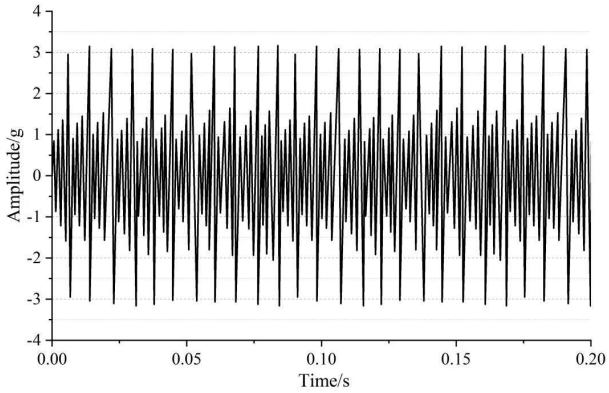

Figure 8: Adding high-frequency harmonic signals to the vibration waveform

Observing the waveforms of normal and abnormal transformer vibration signals reveals that the amplitude of normal transformer vibrations ranges between -2.5g and 2.5g, exhibiting regular fluctuations and periodic changes. Under DC bias vibration conditions, the amplitude is slightly higher. After adding noise to the abnormal signal, the amplitude exhibits irregular fluctuations, with values reaching ±3.7g. When high-frequency harmonic signals are added, the transformer still maintains regular fluctuations, but they occur more frequently and the amplitude increases slightly.

III. B. Analysis of audio signals

After completing the actual measurement and collection of vibration signals from multiple transformers and constructing abnormal data, we conducted a frequency domain analysis to further analyze the signal characteristics. Through Fourier transformation, we converted the time domain waveform into a spectrum diagram to reveal the distribution patterns of the fundamental frequency and harmonic components, providing a basis for subsequent noise removal.

To facilitate the analysis of differences in speech signals, we typically convert the time domain relationship of speech signals into a frequency domain relationship for analysis. The most intuitive way to understand a speech signal is to examine the time-domain plot, which allows one to visually observe the amplitude values at different time points. Therefore, for the speech signals read at different detection points after removing silence, the vertical axis represents the sound pressure level using the level signal. Additionally, to better understand the amplitude-frequency characteristics of the signal, the speech signals measured at different positions were subjected to a Fourier transform. The spectral relationships of the transformer at different detection points are shown in Figure 9.

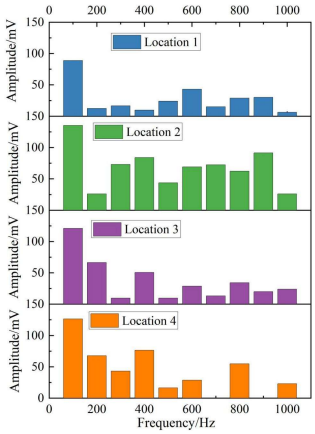

Figure 9: Spectrum diagrams at different positions

As shown in Figure 9, from the spectrum of the detection point, the transformer frequency is mainly concentrated at 100 Hz. In addition to the main frequency, there are also some 100 Hz harmonic components. These harmonic components may be caused by harmonic distortion resulting from nonlinear components inside the transformer, such as magnetic core saturation and iron loss. Furthermore, we must also consider various types of noise that may be present during the audio acquisition process. These noises may originate from electrical interference from the

acquisition equipment itself, electromagnetic interference from the external environment, or instability in the measured signal itself. All of these interference factors may contribute to the generation of harmonic components in the transformer.

III. C. Simulation analysis of transformer vibration signal denoising based on the CEEMD method

To verify the effectiveness of the improved EEMD algorithm (CEEMD) in signal decomposition, this chapter decomposes the simulated signal S1 using the EMD, EEMD, and CEEMD methods, respectively. Then, the CC value is calculated for each IMF component, and the decomposed IMF components are effectively screened by setting a threshold θ. The selected effective IMF components are then recombined to obtain the denoised signal.

III. C. 1) Improving the signal decomposition results of EMDD

In the parameter configuration of CEEMD, there are three main parameters: noise standard deviation (NSD), number of noise additions (NR), and maximum iteration count (MaxIter). These parameters are typically selected based on prior experience, with NSD generally chosen between 0 and 1, NR between 50 and 200, and MaxIter typically set to a larger value. Since CEEMD has not been applied to transformer vibration signals and the noise reduction effectiveness of this method is strongly correlated with the NSD and NR parameters, it is not advisable to directly select parameters based on experience. To select parameters suitable for transformer vibration signals and achieve better noise reduction results, this experiment employs the control variable method to select NSD and NR. After calculation, the CEEMD parameters selected for transformer vibration signals in this experiment are: NSD set to 0.3, NR set to 120, and MaxIter set to 550. The simulation signal S1 is shown in Figure 10, and the results of the 10 IMF components obtained after decomposition are shown in Figures 11 and 12.

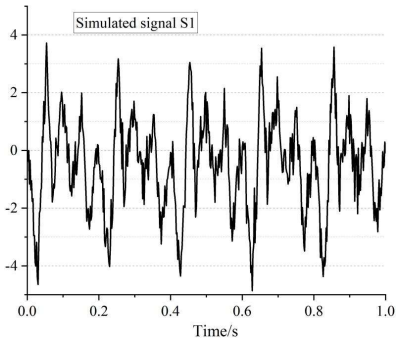

Figure 10: Simulated signal S1

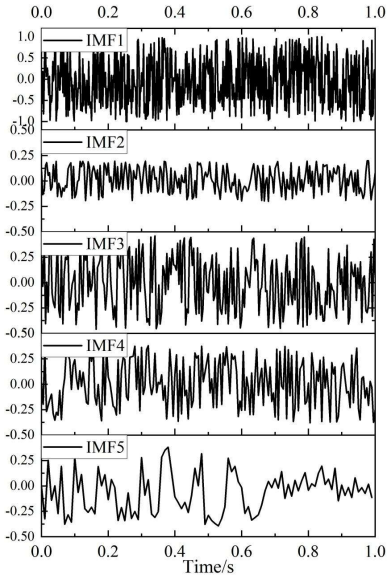

Figure 11: IMF1-IMF5 component results

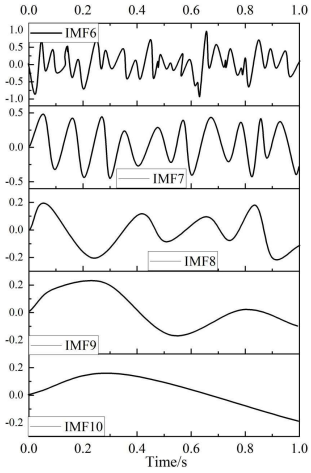

Figure 12: IMF6-IMF10 component results

As can be seen, the CEEMD method decomposes the signal into 10 IMF components. The more components there are, the more detailed the decomposition and the more information it contains. Among these, the noise in the original signal is more likely to be separated out, which not only facilitates signal denoising but also makes it easier to extract signal features in subsequent steps. Overall, as the number of IMFs increases, the corresponding frequencies decrease. Typically, high-frequency IMF components are primarily composed of noise, while low-frequency IMF components primarily consist of useful signals. Therefore, by selecting the IMF components decomposed by CEEMD, effective information can be extracted, and some noise can be removed.

CEEMD decomposition does not exhibit modal aliasing. This indicates that the CEEMD method can effectively avoid the occurrence of modal aliasing. By comparing the changes in each IMF component of CEEMD, we find that the frequency changes between different IMF components are very distinct, further demonstrating that CEEMD can effectively suppress modal aliasing. CEEMD decomposition first obtains the first-order IMF, then calculates the final first-order IMF through overall averaging, followed by calculations for the remaining components. Through this calculation process, the CEEMD method effectively addresses the issues of white noise transfer from high to low frequencies, noise propagation, and residual noise. Therefore, CEEMD decomposition can effectively suppress modal aliasing and residual noise issues.

III. C. 2) Comparison of the computational speeds of the EEMD and CEEMD algorithms

To better validate the efficiency of the CEEMD algorithm in signal decomposition, box plots of the number of iterations of IMF were used to compare the computational speeds of the EEMD and CEEMD algorithms. The box plot results for the two algorithms are shown in Figures 13 and 14, respectively. The vertical axis represents the number of iterations, and the horizontal axis represents the IMF components. This box plot illustrates the number of iterations required to decompose different components using different decomposition methods.

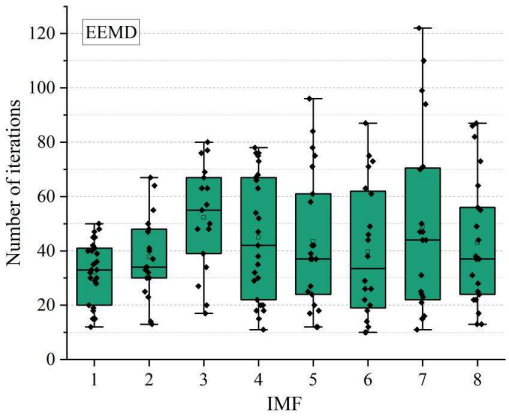

Figure 13: The number of iterations of IMF under the EEMD algorithm

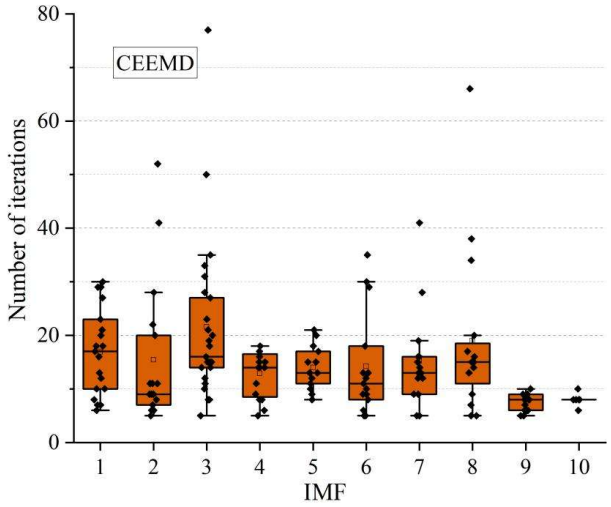

Figure 14: The number of iterations of IMF under the CEEMD algorithm

As can be seen from the figure, EEMD decomposes only eight components, and for each IMF selection, the maximum number of iterations for the EEMD method is 122, while for the CEEMD method it is 76. The average number of iterations for the two methods is 42 and 15, respectively, with the CEEMD method requiring nearly one-third less computational effort than the EEMD method. This also means that the CEEMD method can reduce operation time and improve the efficiency of signal decomposition.

III. C. 3) Comparison of Different Noise Reduction Methods

Noise reduction was performed on the simulated noisy signals using different noise reduction methods, and the noise reduction indicators are shown in Table 1.

As shown in Table 1, in terms of signal-to-noise ratio (SNR), CEEMD performs the best with an SNR of 18.11 dB, significantly higher than EMD's 13.34 dB and EEMD's 14.44 dB. Additionally, its SNR improvement value (SNRimp) of 13.88 dB also far exceeds that of other methods. In terms of error, CEEMD has the lowest mean squared error (MSE) of 0.0177 and root mean squared error (RMSE) of 0.1258, indicating minimal signal distortion. Although wavelet denoising achieves a high SNR of 16.37 dB and relatively low errors (MSE and RMSE of 0.0216 and 0.1499, respectively), the mother wavelet and decomposition levels must be manually selected, and improper threshold selection can cause signal distortion, directly affecting denoising performance. The signals obtained after EMD and EEMD denoising differ significantly from the original signals. The poor denoising effect of EMD is due to modal overlap in the decomposition results. Mode overlap causes the properties of components to become similar, affecting component selection and thereby degrading noise reduction performance. Although the EEMD method addresses mode overlap during EMD decomposition by adding white noise, it still faces the issue of residual noise in the decomposed IMF components. Therefore, EEMD also has certain limitations in noise reduction. The improved CEEMD method used in this paper addresses the issue of residual noise by using weighted averaging to offset the residual noise in the components. It can efficiently and meticulously decompose signals and is suitable for noise reduction in vibration signals.

Table 1: Different methods for noise reduction indicators

	SNR/dB	SNR_{imp}/dB	MSE	RMSE	PDR/%
Wavelet denoising	16.37	11.22	0.0216	0.1499	14.38
EMD	13.34	8.54	0.0508	0.2024	22.38
EEMD	14.44	10.25	0.0369	0.1695	18.66
CEEMD	18.11	13.88	0.0177	0.1258	12.02

IV. Identification and analysis of typical faults in power transformers

Based on the acquisition of high-fidelity denoised acoustic signals, this chapter will focus on the ultimate goal of the research—the intelligent identification and classification of typical mechanical faults in power transformers. Utilizing the SSAE-IELM diagnostic model constructed in Chapter 2, combined with the acoustic signature dataset that has

undergone preprocessing and feature extraction, this study will thoroughly investigate the acoustic characteristic differences among various fault types and systematically evaluate the diagnostic performance of the model, thereby completing the critical validation process from “signal denoising” to “condition assessment.”

IV. A. Sources of experimental data

During the operation of power transformers, the probability of faults such as short-circuit impacts is relatively low, which can easily lead to an imbalance in the number of samples. Based on the acoustic fingerprint data provided in the previous section, this paper separately plots the time-frequency spectra and Mel time-frequency spectra of normal and fault samples. Additionally, basic data augmentation and Mixup data augmentation were applied to the obtained spectra. The number of samples for the three fault types—normal state, short-circuit surge, DC bias, and partial discharge—are 2,000, 1,500, 1,500, and 1,000, respectively. Among these, 3/4 of the samples are used for model training, and 1/4 are used for testing. To verify the accuracy of the expanded data, the original data is added to the test set for classification identification.

IV. B. Analysis of fault type detection in different models

The constructed datasets were imported into the CNN model for training. The model was built using the deep learning framework TensorFlow in a Python environment. The computing platform was configured with an Intel i7-8750H CPU running at 2.20 GHz, 16 GB of memory, and a 64-bit Windows 10 operating system. The number of iterations was set to 50, and the number of units in the fully connected layer was set to 60.

The comparison models include the standard basic model based on the CNN deep learning algorithm, the ACO-CNN and GWO-CNN models optimized by ACO and GWO, respectively, and the SSAE-IELM transformer fault detection model based on stacked sparse autoencoders and incremental extreme learning machines proposed in this paper.

IV. B. 1) Diagnostic accuracy of different models

The diagnostic accuracy rates of the four models are shown in Figures 15, 16, 17, and 18, respectively.

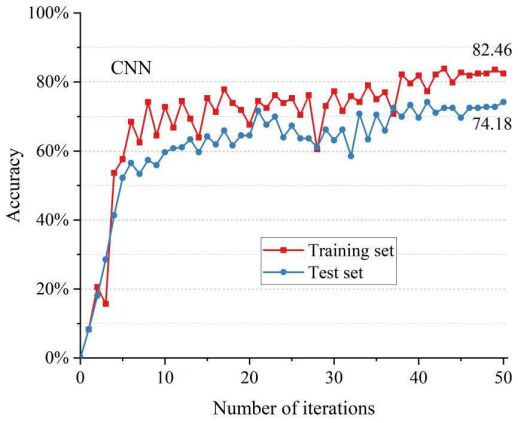

Figure 15: Diagnostic accuracy under the CNN model

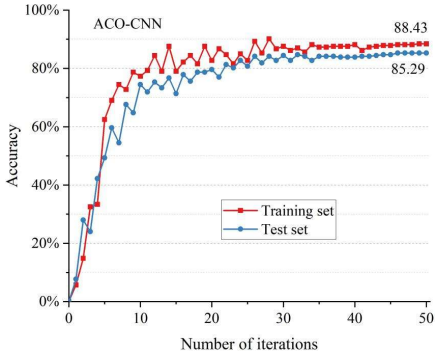

Figure 16: Diagnostic accuracy under the ACO-CNN model

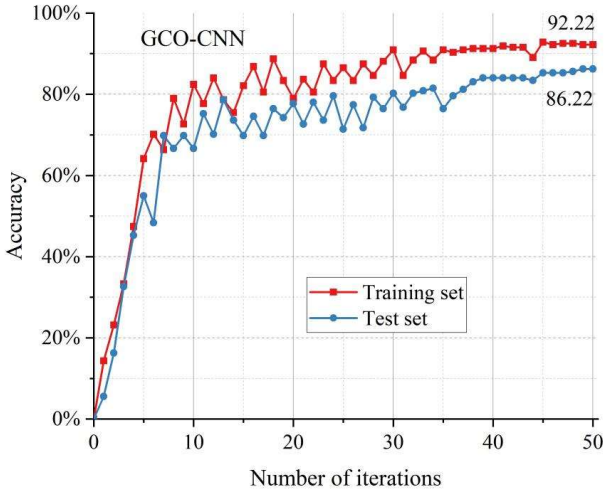

Figure 17: Diagnostic accuracy under the GCO-CNN model

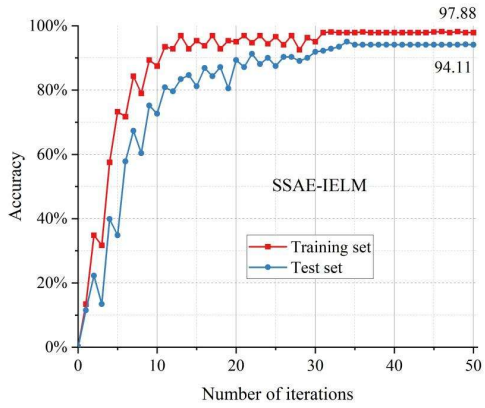

Figure 18: Diagnostic accuracy under the SSAE-IELM model

As shown in the figure above, the SSAE-IELM model achieves the highest diagnostic accuracy. On the training set, it reaches a stable state by the 31st iteration with an accuracy rate of 97.88%, and on the test set with fewer samples, it achieves 94.11%; Under the CNN model, stability was not achieved until the 44th iteration, with an accuracy rate of 82.46%. After optimization using ACO and GCO, the accuracy rates of the CNN model eventually stabilized at 88.43% and 92.22%, respectively.

IV. B. 2) Fault Classification Confusion Analysis

The confusion matrix was used to measure the classification accuracy of each model. The classification results of the four models are shown in Figures 19, 20, 21, and 22, respectively.

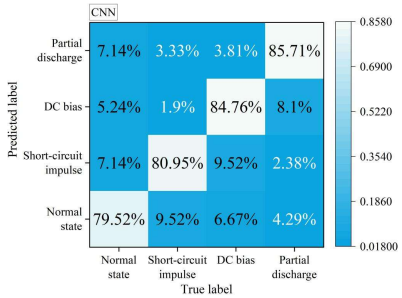

Figure 19: Fault Classification Confusion Analysis Matrix of CNN

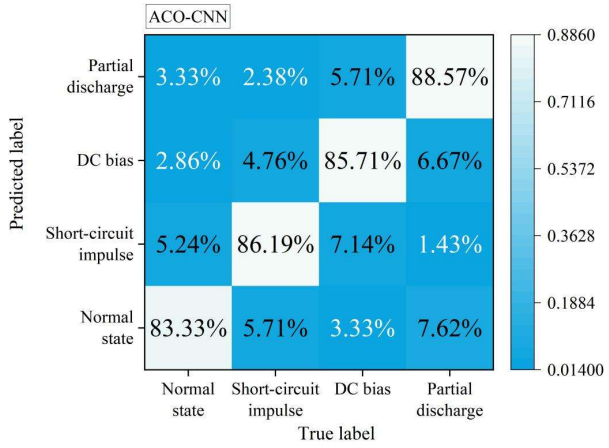

Figure 20: Fault Classification Confusion Analysis Matrix of ACO-CNN

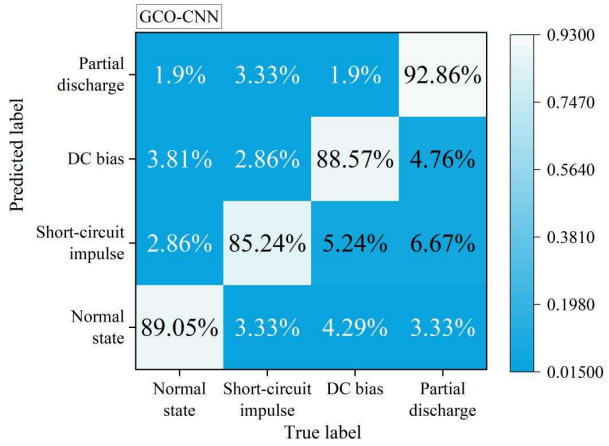

Figure 21: Fault Classification Confusion Analysis Matrix of GCO-CNN

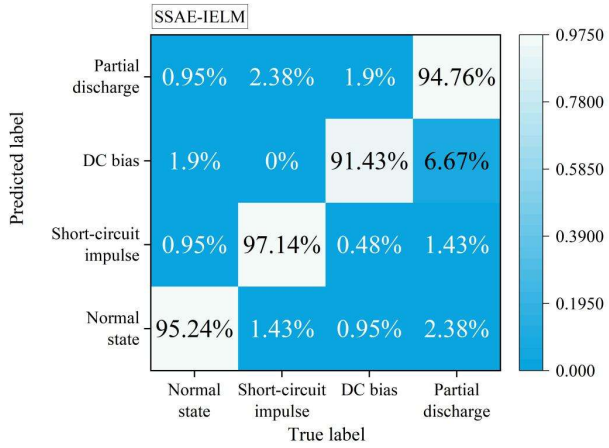

Figure 22: Fault Classification Confusion Analysis Matrix of SSAE-IELM

It can be seen that the SSAE-IELM model performs the best, achieving an accuracy rate of 95.24% in normal state recognition, significantly higher than the 79.52% of CNN, 83.33% of ACO-CNN, and 89.05% of GCO-CNN. For short-circuit impact faults, its recognition rate reaches 97.14%, far superior to other models (CNN: 80.95%, ACO-CNN: 86.19%, GCO-CNN: 85.24%); for DC bias fault recognition, its accuracy rate is 91.43%, also outperforming CNN (84.76%) and ACO-CNN (85.71%), though slightly lower than GCO-CNN (88.57%); For partial discharge faults, its recognition rate of 94.76% is the highest among all models (CNN: 85.71%, ACO-CNN: 88.57%, GCO-CNN: 92.86%). Additionally, the SSAE-IELM model has the lowest misclassification rates overall, such as

misclassifying normal states as short-circuit impacts at only 0.95% and misclassifying DC bias as partial discharges at only 1.90%. In contrast, other models (especially the base CNN) exhibit more significant inter-category confusion. For example, the CNN misclassifies normal states as the other three fault categories at a combined rate of 20.48%, and all fault categories exhibit varying degrees of misclassification spread. For instance, 9.52% of short-circuit impacts are misclassified as normal states. This indicates that the SSAE-IELM model has a significant advantage and higher reliability in distinguishing various transformer states, particularly between normal states and short-circuit impact faults.

V. Conclusion

This study established a transformer condition monitoring method based on voiceprint signal analysis. Through theoretical analysis, system design, and experimental verification, the following conclusions were drawn.

(1) The multi-channel synchronous acquisition system successfully obtained actual measurement data from a 110kV transformer. Under normal operating conditions, the vibration amplitude was stable at -2.5g to 2.5g. Under DC bias conditions, the amplitude increased, and under noise interference, the amplitude of abnormal signals reached ±3.7g.

(2) The improved EEMD algorithm demonstrated significant noise reduction performance, with the signal-to-noise ratio (SNR) improved to 18.11 dB (a 26% increase over EEMD), the mean squared error reduced to 0.0177, and computational efficiency enhanced by 64.29%, effectively suppressing harmonic and white noise interference.

(3) The SSAE-IELM model demonstrates outstanding diagnostic advantages, with an overall accuracy rate of 94.11% and a training set accuracy rate of 97.88%, significantly outperforming CNN (82.46%), ACO-CNN (88.43%), and GCO-CNN (92.22%).

(4) The confusion matrix shows that the recognition rate for normal states is 95.24%, the recognition rate for short-circuit impacts is 97.14%, and the recognition rate for partial discharges is 94.76%. The misclassification rate between categories is below 2.38%, such as 0.95% for normal → short-circuit.

This method addresses the challenge of acoustic fingerprint diagnosis in the complex electromagnetic environment of urban substations, providing a high-precision, high-efficiency technical solution for non-invasive condition monitoring of transformers.

Funding

This research was supported by the Science and Technology Project Fund of State Grid Shanxi Electric Power Company: Research on Potential Fault Field Perception and Analysis Technology for Transformers Based on Small Sample Parameters (5205M024000J).

References

[1] Silva-Ortega, J., Ortíz, J., & Candelo-Becerra, J. E. (2024). A New Method to Assess the Reliability and Security of Urban Electrical Substations. Electricity, 5(4), 991-1007.

[2] Jun, L., Li, L., Yongxiang, Z., Zhigang, C., & Xiaopeng, F. (2021). Annoyance evaluation of noise emitted by urban substation. Journal of Low Frequency Noise, Vibration and Active Control, 40(4), 2106-2114.

[3] Lei, H., & Singh, C. (2015). Power system reliability evaluation considering cyber-malfunctions in substations. Electric Power Systems Research, 129, 160-169.

[4] Waleed, A., Virk, U. S., Riaz, M. T., Mehmood, S. B., Ahmad, S., Javed, M. R., & Raza, A. (2019). Effectiveness and comparison of digital substations over conventional substations. Advances in Science, Technology and Engineering Systems Journal, 4(4), 431-439.

[5] Skuza, A., Ziemianek, S., & Suproniuk, M. (2022). Power System Division—Certain Issues Associated with Shaping Commutation Strategies in Power Substations. Energies, 15(19), 7293.

[6] Kovačev, N., Gavrić, M., & Lendák, I. (2023). Algorithm for visualizing substation areas in electric power systems. Expert Systems with Applications, 212, 118733.

[7] An, B., Oh, J., & Park, T. (2025). A Study on the Optimal Configuration of Offshore Substation Transformers. Energies, 18(12), 3076.

[8] Popa, C. (2020). Impact of substations equipment to the environment. International Journal of Global Warming, 21(2), 155-172.

[9] Parise, G., Parise, L., Martufi, M., Su, C. L., Chavdarian, P. B., & Panetta, S. A. (2016). Neutral grounding in MV transformers substations for cranes service. IEEE Transactions on Industry Applications, 52(3), 2070-2076.

[10] Humayun, M., Sousa, B. J. O., Safdarian, A., Ali, M., Degefa, M. Z., Lehtonen, M., & Fotuhi-Firuzabad, M. (2015). Optimal capacity management of substation transformers over long-run. IEEE Transactions on Power Systems, 31(1), 632-641.

[11] Lagoeiro, H., Davies, G., Marques, C., & Maidment, G. (2023). Heat recovery opportunities from electrical substation transformers. Energy Reports, 10, 2931-2943.

[12] Schmitz, W. I., Feil, D. L., Canha, L. N., Abaide, A. R., Marchesan, T. B., & Carraro, R. (2018). Operational vulnerability indicator for prioritization and replacement of power transformers in substation. International Journal of Electrical Power & Energy Systems, 102, 60-70.

[13] Xie, B., Zhao, D., & Hong, T. (2020). Transformer monitoring and protection in dynamic power systems–a review. Frontiers in Energy Research, 8, 150.

[14] Hernandez, M. D. P. C., & Labib, A. (2017). Selecting a condition monitoring system for enhancing effectiveness of power transformer maintenance. Journal of Quality in Maintenance Engineering, 23(4), 400-414.

[15] Chandran, L. R., Babu, G. A., Nair, M. G., & Ilango, K. (2021). A review on status monitoring techniques of transformer and a case study on loss of life calculation of distribution transformers. Materials Today: Proceedings, 46, 4659-4666.
[16] Zhou, H., Lu, L., Wang, G., & Su, Z. (2024). A new validity detection method of online status monitoring data for power transformer. Ieee Access, 12, 16095-16104.
[17] Barakat, A., Naqra, A., & Hussian, A. (2024). Measuring the Accuracy of A Voiceprint Analysis System Designed by Applying the Euclidean Distance Function and Genetic Algorithm. SSRG International Journal of Electrical and Electronics Engineering, 11(3).
[18] Babu, A., Raoul, E., Kassahun, G., Dufour, I., Mandal, D., & Thuau, D. (2024). Programmable Polymeric-Interface for Voiceprint Biometrics. Advanced Materials Technologies, 9(4), 2301551.
[19] SONG, J., XUAN, D., WANG, W., SUN, F., & SONG, Y. (2024). Operation and maintenance detection technology for energy storage transformers based on voiceprint features. Energy Storage Science and Technology, 13(8), 2758.
[20] Wang, J., Zhao, Z., Zhu, J., Li, X., Dong, F., & Wan, S. (2023). Improved support vector machine for voiceprint diagnosis of typical faults in power transformers. Machines, 11(5), 539.
[21] Peng, J., Ma, Y., Ye, H., Che, X., Li, S., & Ai, B. (2025). Voiceprint recognition method of transformer based on LBT-ODF and MVN. Journal of Measurements in Engineering.
[22] SHEKAR, K., MADHAVI, B., THRISHA, G., KRISHNA, T. G., & ARUNA, M. (2024). ADVANCED DISTRIBUTION TRANSFORMER LOAD MONITORING AND CONTROLLING BY USING GSM MODEM. MATERIAL SCIENCE, 23(04).
[23] Tan, X., Zhou, F., Li, W., Ao, G., Xu, X., & Yang, L. (2024). Surface Wear Monitoring System of Industrial Transformer Tap-Changer Contacts by Using Voice Signal. Coatings, 14(5), 583.
[24] Lv, Z., Yang, D., & Wei, B. (2024). Technical analysis of transformer vowel print fault diagnosis based on CNN-LSTM network. International Journal of COMADEM, 27(1).
[25] Xia, Y., He, Y., Kang, B., Wang, Y., Dong, X., & Zhang, Z. (2024, December). Research and application of MFCC-LSTM based on improved ZOA algorithm to optimize transformer voice-print diagnosis. In 2024 4th International Conference on Electrical Engineering and Control Science (IC2ECS) (pp. 559-563). IEEE.
[26] Liu, G., Gao, L., Yu, L., & Yang, W. (2024, July). Research on Transformer Fault Diagnosis Based on Voiceprint Signal. In Journal of Physics: Conference Series (Vol. 2774, No. 1, p. 012052). IOP Publishing.
[27] Wang, Y., Dong, W., Azan, D., Wang, X., Wufuer, R., & Wang, H. (2024, November). Voiceprint State Identification of Power Transformers Based on Probabilistic Neural Network. In 2024 6th International Conference on Artificial Intelligence and Computer Applications (ICAICA) (pp. 154-158). IEEE.
[28] Yu, Z., Wei, Y., Niu, B., & Zhang, X. (2024). Automatic condition monitoring and fault diagnosis system for power transformers based on voiceprint recognition. IEEE Transactions on Instrumentation and Measurement.
[29] Yu, D., Zhang, W., & Wang, H. (2023). Research on transformer voiceprint anomaly detection based on data-driven. Energies, 16(5), 2151.
[30] Cai, R., Wang, Q., Hou, Y., & Liu, H. (2021, November). Event monitoring of transformer discharge sounds based on voiceprint. In Journal of Physics: Conference Series (Vol. 2078, No. 1, p. 012066). IOP Publishing.
[31] He, P., Xu, H., Yin, L., Wang, L., & Zhu, L. (2021, December). Power Transformer Voiceprint Operation State Monitoring Considering Sample Unbalance. In Journal of Physics: Conference Series (Vol. 2137, No. 1, p. 012007). IOP Publishing.
[32] Wang, L., Fan, Y., Yang, X., Li, B., Li, W., Xue, J., ... & Guo, X. (2022, October). Exploration of Transformer Operation and Maintenance Technology and Realization of Transformer Condition Monitoring System. In Annual Conference on Power System and Automation in Chinese Universities (pp. 816-825). Singapore: Springer Nature Singapore.
[33] Zhang, K., Lu, H., Han, S., & Zhao, X. (2025). A Novel Fault Diagnosis Method for Power Transformers Based on Voiceprint Recognition Considering Multi-type Noises. IEEE Transactions on Instrumentation and Measurement.
[34] Lu, H., Liang, D., Zhang, Y., Gu, L., Yin, W., & Xiao, Y. (2024, November). Research on Transformer Fault Diagnosis Method Based on Small Sample Voiceprint Recognition Technology. In 2024 IEEE 8th Conference on Energy Internet and Energy System Integration (EI2) (pp. 5286-5290). IEEE.
[35] Wan, S., Dong, F., Zhang, X., Wu, W., & Li, J. (2023). Fault voiceprint signal diagnosis method of power transformer based on Mixup data enhancement. Sensors, 23(6), 3341.
[36] Ma, G., Wang, Y., Qin, W., Zhou, H., Yan, C., Jiang, J., & Ju, Y. (2021). Optical sensors for power transformer monitoring: A review. High Voltage, 6(3), 367-386.
[37] Wenhua, W., Rui, C., Yu, C., Xu, Z., & Yongbing, X. (2024). Research on standardization of power transformer monitoring and early warning based on multi-source data. Frontiers in Energy Research, 12, 1442299.
[38] Cui, J., Kuang, W., Geng, K., & Jiao, P. (2025). Intelligent fault diagnosis and operation condition monitoring of transformer based on multi-source data fusion and mining. Scientific Reports, 15(1), 7606.
[39] Wang, W., Chen, Q., Qiao, S., Cheng, Y., & Ji, X. (2024, May). A Transformer Warning Method Based on Pattern Recognition and Statistical Analysis. In 2024 IEEE 6th Advanced Information Management, Communicates, Electronic and Automation Control Conference (IMCEC) (Vol. 6, pp. 1481-1486). IEEE.
[40] Dubey, P. K., Singh, B., Patel, D. K., & Kumar, R. (2025). Review of Transformer Health Monitoring System and Fault Detection. International Journal of Sciences and Innovation Engineering, 2(6), 209-223.